Imaging Elemental Events of Store-operated Ca^{2+} Entry in Invading Cancer Cells with Plasmalemmal Targeted Sensors

Fujian Lu[1*], Jianwei Sun[2,3*], Qiaoxia Zheng, Jinghang Li[1], Yuanzhao Hu[3], Peng Yu[1], Huifang He[4], Yan Zhao[1], Xianhua Wang[1], Shengyu Yang[2,4#], Heping Cheng[1#]

[1]State Key Laboratory of Membrane Biology, Institute of Molecular Medicine, Peking-Tsinghua Center for Life Sciences, Peking University, Beijing 100871, China

[2]Department of Cellular and Molecular Physiology, Penn State College of Medicine, Hershey, PA 17033, USA

[3]State Key Laboratory for Conservation and Utilization of Bio-Resources in Yunnan, Center for Life Sciences, School of Life Sciences, Yunnan University, Kunming, 650091, China.

[4]Department of Tumor Biology, H. Lee Moffitt Cancer Center, Tampa, FL 33612, USA

Key Words: Ca^{2+} Biosensor, Store-operated Ca^{2+} Entry, Ca^{2+} Glows, Pyk2, Invasion

***These authors contributed equally to this work.**

#To whom correspondence should be addressed: sxy99@psu.edu or chengp@pku.edu.cn

JCS Advance Online Article. Posted on 27 February 2019

Summary Statement

Elemental Ca^{2+} signals of store-operated Ca^{2+} entry are visualized in native cancer and endothelial cells by newly developed plasmalemmal targeted sensors, and are critical for invasion via regulating Pyk2-Src pathway.

Abstract

STIM1- and Orai1-mediated store-operated Ca^{2+} entry (SOCE) constitutes the major Ca^{2+} influx in almost all electrically non-excitable cells. However, little is known about the spatiotemporal organization at the elementary level. Here, we developed Orai1-tethered or palmitoylated biosensor GCaMP6f to report subplasmalemmal Ca^{2+} signals. We visualized spontaneous discrete and long-lasting transients ("Ca^{2+} glows") arising from STIM1-Orai1 in invading melanoma cells. Ca^{2+} glows occurred preferentially in single invadopodia and at sites near cell periphery under resting conditions. Re-addition of external Ca^{2+} after store depletion elicited spatially synchronous Ca^{2+} glows followed by high-rate discharge of asynchronous local events. Knockout of STIM1 or expression of the dominant-negative Orai1-E106A mutant markedly decreased Ca^{2+} glow frequency, diminished global SOCE and attenuated invadopodial formation. Functionally, invadopodial Ca^{2+} glows provided high Ca^{2+} microdomains to locally activate Ca^{2+}/calmodulin-dependent Pyk2, which initiates the SOCE-Pyk2-Src signaling cascade required for invasion. Overall, the discovery of elemental Ca^{2+} signals of SOCE not only unveils a previously unappreciated gating mode of STIM1-Orai1 channels *in situ*, but underscores a critical role of the spatiotemporal dynamics of SOCE in orchestrating complex cell behaviors such as invasion.

Introduction

Ca^{2+} is a remarkably versatile second messenger that controls a wide range of physiological and pathophysiological processes (Berridge et al., 2003). Cytosolic Ca^{2+} is tightly controlled by an elaborate system consisting of channels, pumps, and exchangers as well as buffers. The spatial and temporal organization of cytosolic and organellar Ca^{2+} is also crucial for the speed, specificity, and robustness of Ca^{2+} signaling (Berridge et al., 2003; Cheng and Lederer, 2008). Among a plethora of Ca^{2+} entry pathways, store-operated Ca^{2+} channels (SOCs) are the predominant mechanism responsible for replenishing the endoplasmic reticulum (ER) Ca^{2+} store (Parekh and Putney, 2005) in electrically non-excitable cells. As well, SOCE has been described in some excitable cells (Chen and Sanderson, 2017; Feldman et al., 2017; Wei-LaPierre et al., 2013). The ER-resident Ca^{2+} sensor, stromal interacting molecule (STIM), and the plasma membrane (PM) pore-forming subunit Orai, are the two critical components of store-operated Ca^{2+} entry (SOCE). Upon depletion of the ER Ca^{2+} store, STIM1 oligomerizes and translocates to the ER-PM junctions to cluster and activate Orai1 channels and Ca^{2+} influx.

To date, little is known about the spatiotemporal organization of SOCE at the elementary level, In particular, it is not clear whether SOCE comprises elementary Ca^{2+} signals that are similar to Ca^{2+} sparks (Cheng et al., 1993) and Ca^{2+} puffs (Yao and Parker, 1994) for stored Ca^{2+} release mediated by ryanodine receptors and inositol 1, 4, 5-triphosphate receptors. It is believed that Ca^{2+} concentration microdomains are confined to tens of nanometers within the open mouth of activated SOC channels (Hogan, 2015), and the clustering of Orai1 proteins significantly enhances the signaling downstream of SOCE (Samanta et al., 2015). Therefore, detection of such STIM1-Orai puncta-mediated Ca^{2+} microdomains could provide insightful

information into how the spatiotemporal dynamics of SOCE orchestrates downstream signaling, as well as check the veracity of models for STIM1-Orai1 gating in the cluster.

STIM1 and Orai1 have been increasingly implicated in cancer and are reported to be essential for cancer cell migration and invasion (Sun et al., 2014). Invadopodia, the invasion machinery, are proteolytic membrane protrusions used by malignant cells to remodel the extracellular matrix and to facilitate metastatic dissemination (Murphy and Courtneidge, 2011). The invadopodium consists of an actin-rich core surrounded by a ring of adhesive protein complexes (Gimona et al., 2008; Linder, 2007). The assembly of invadopodia is stimulated in response to pro-invasion cues in the tumor microenvironment (Murphy and Courtneidge, 2011), which activate the non-receptor tyrosine kinase Src to initiate the nucleation of the invadopodial F-actin core (Gimona et al., 2008). Here, we mainly used a cancer cell model to investigate the spatiotemporal Ca^{2+} dynamics of SOCE in intact cells, to illustrate its interplay with subcellular morphological structures, and to explore the cellular and molecular mechanisms by which SOCE controls downstream signaling.

By fusing the genetically encoded Ca^{2+} indicator GCaMP6f to the N-terminus of the Orai1 channel or attaching the palmitoylation sequence of the human GAP43 protein to GCaMP6f, we developed plasmalemma-targeted biosensors to preferentially report Ca^{2+} influx. We discovered spontaneous, long-lasting Ca^{2+} transients confined to single invadopodia as well as discrete sites at the cell periphery of invading melanoma cells. Such local Ca^{2+} transients, dubbed "Ca^{2+} glows", constitute elementary events of SOCE mediated by STIM1 and Orai1 clusters. Similar Ca^{2+} glows of STIM1 and Orai1 origin were found in human umbilical vein endothelial cells (HUVECs). We further demonstrated that, in the cancer cell model,

invadopodial Ca^{2+} glows play an important role in orchestrating local Pyk2 and Src activation to signal cancer cell invasion.

Results

Targeting GCaMP6f to the Plasma Membrane to Report Subplasmalemmal Ca^{2+}

Upon depletion of the ER Ca^{2+} store, STIM1 translocates and accumulates in regions of the ER-PM junction, where it clusters Orai1 through physical contact to form structures commonly referred to as "puncta" (Liou et al., 2005; Wu et al., 2006). STIM1 also provides the signal that activates the apposed Orai1, a highly Ca^{2+}-selective channel with extremely small single-channel conductance (Prakriya and Lewis, 2015). We reckoned that targeting a Ca^{2+} sensor to the microdomain of the Orai1 channel mouth would enable us to investigate how the STIM-Orai1 puncta operate in live cells. We therefore fused the genetically encoded Ca^{2+} probe GCaMP6f to the N terminus of Orai1 adjacent to the transmembrane domain (**Fig. 1A**). It has been reported that protein fusion in this region does not alter the assembly, trafficking, and activity of SOCs (Li et al., 2007; Park et al., 2009; Zhou et al., 2016). The Ca^{2+} biosensor GCaMP6f was chosen because of its demonstrated capabilities in resolving ryanodine receptor-mediated Ca^{2+} sparks in heart cells (Shang et al., 2014) and Ca^{2+} transients elicited by single action potentials in neurons (Chen et al., 2013). As an alternative strategy to probe subsurface Ca^{2+} without altering the stoichiometry of STIM1 and Orai1, we generated another targeted Ca^{2+} sensor, PM-GCaMP6f, by attaching the palmitoylation sequence of the human GAP43 protein to the N terminus of GCaMP6f (Varnai et al., 2006).

To investigate the spatiotemporal properties of SOCE, we used the highly invasive WM793 human melanoma cell as a model system of non-excitable cells. WM793 cells plated on gelatin-coated coverslips were first infected with GCaMP6f-Orai1 adenovirus for 36 h. After stimulation with 10% fetal bovine serum (FBS), serum-starved WM793 cells start to assemble actin-rich protrusion structures and form invadopodia arrays, usually beneath the nucleus region. Functional invadopodia secrete proteases to degrade the extracellular matrix, producing pits and holes in the thin tetramethylrhodamine (TRITC)-gelatin coating, which were visualized by the loss of TRITC fluorescence (**Fig. 1B**). Confocal imaging revealed that the invadopodia were intensely stained with GCaMP6f-Orai1, giving rise to a ring-like structure wrapping around the actin-rich invadopodial core labeled by Lifeact-mApple (**Fig. 1B upper panel**) or surrounding the TRITC-free pits and holes in the gelatin coat as seen from both 2D and 3D z-stack images (**Fig. 1B lower panel**). Intensely fluorescent puncta were also evident at sites near the cell periphery. Because a similar pattern of distribution was evident with PM-GCaMP6f (**Fig. S1A**), the appearance of inhomogeneity was likely due to unevenness of the plasma membrane seen in the confocal optical section (e.g., the ring structure at invadopodia could be explained by the vertical dimension of the plasma membrane at these loci). Thus, both of the membrane-targeted Ca^{2+} biosensors, GCaMP6f-Orai1 and PM-GCaMP6f, would enable the investigation of SOCE activity at single-invadopodium resolution.

To determine whether the expression of GCaMP6f-Orai1 altered SOCE due to a change in the stoichiometry of STIM1 and Orai1, we measured the expression level of GCaM6f-Orai1 and found that it was ~30% of that of endogenous Orai1 in WM793 cells, without an appreciable compensatory change in STIM1 expression (**Fig. 1C**). Functionally, GCaM6f-Orai1 expression did not alter the magnitude of SOCE induced by Ca^{2+} re-addition after ER depletion (**Fig. 1D**),

and neither did it affect the number of invadopodia in WM793 cells (**Fig. 1E**), indicating that perturbation of SOCE by GCaMP6f-Orai1 expression, if any, is negligible. Further, to appraise the relative sensitivity of the membrane-targeted biosensors to Ca^{2+} influx *versus* Ca^{2+} release, we made dual-indicator measurements using GCaMP6f-Orai1 and Rhod4; the latter is diffusible in the cytosol. We found that, while global SOCE led to similar fold-increases of fluorescence of the two indicators, thapsigargin (TG)-induced ER Ca^{2+} release elicited a fold change of GCaMP6f-Orai1 fluorescence that was merely 50% of that of Rhod4 (**Fig. S2A**). This result suggests that the membrane-targeted Ca^{2+} biosensor preferentially reports subplasmalemmal Ca^{2+} and is relatively insensitive to Ca^{2+} release from the ER, which is in agreement with a previous report (Dynes et al., 2016). In the rest of the study, we opted to use GCaMP6f-Orai1 as the Ca^{2+} biosensor in most experiments, and PM-GCaMP6f in a subset of experiments mainly for the purpose of validation.

Spontaneous Ca^{2+} Glows in Invading Melanoma Cells

In WM793 cells expressing GCaMP6f-Orai1, we used time-lapse confocal imaging to acquire 400 consecutive images at 5-s intervals. Discrete, sudden, and transient GCaMP6f-Orai1 fluorescence increases arose spontaneously from the biosensor-labeled invadopodia (**Fig. 2A, Video 1**). Individual transients were confined to single invadopodia, with no sign of propagation into adjacent invadopodia or extra-invadopodial areas (**Fig. 2A upper panel**). Their full duration at half maximum (FDHM) lasted up to tens of seconds with an average value of 11.5 s (**Fig. 2A** and **2D**). Transient increases of GCaMP6f-Orai1 fluorescence were also found at discrete sites at the cell periphery (**Fig. S3A**). We named them Ca^{2+} glows because of their exceptionally long duration. On average, the rate of occurrence was 0.5 events/min/cell for invadopodial Ca^{2+} glows and 0.24 events/min/cell for peripheral Ca^{2+} glows. The spatial size of invadopodial Ca^{2+}

glows ranged from 0.5 to 16.5 μm^2 with an average of 3.4 μm^2 (**Fig. 2B**). The histogram of invadopodial glow amplitude displayed a broad distribution ranging from 0.1 to 4.36 ($\Delta F/F_0$), with an average 0.63-fold increase of GCaMP6f-Orai1 fluorescence (**Fig. 2C**). Invadopodial Ca^{2+} glows exhibited highly variable kinetics: oftentimes a rapid rise was followed by either a spiky peak or a prolonged plateau; stepwise fluctuations were sometimes evident in the rise or the plateau phase; likewise, their termination also manifested different patterns, with an abrupt fall or a gradual decline, suggestive of complex gating behavior of the underlying Ca^{2+} channels. To resolve possible faster Ca^{2+} dynamics, we applied linescan imaging at 3.78-ms resolution, and were able to identify substructures lasting <5 s among long-lasting Ca^{2+} glows, but failed to detect any sub-second events (**Fig. 2E** and **2F**). Therefore, Ca^{2+} glows are kinetically distinctive compared to known elementary Ca^{2+} signaling events, such as Ca^{2+} sparks originating from ryanodine receptor Ca^{2+} release channels (~20 ms) in muscles (Cheng and Lederer, 2008), Ca^{2+} puffs from the inositol 1, 4, 5-trisphosphate receptor (IP_3R) Ca^{2+} release channels (~300 ms) in non-excitable cells (Smith et al., 2009), and Ca^{2+} flickers from TRPM7 and coupled activation of IP_3Rs (~500 ms) in WI-38 cells undergoing directional movement (Wei et al., 2012). Notably, peripheral Ca^{2+} glows, such as those in filopodia, exhibited comparable, though not identical, amplitude ($\Delta F/F_0$, 1.26) (**Fig. S3B**), duration (FDHM, 8.44 s) (**Fig. S3C**), and spatial size (12.3 μm^2) (**Fig. S3D**). Taken together, invadopodial and peripheral Ca^{2+} glows reflect previously unappreciated local Ca^{2+} signaling events in invading melanoma cells.

Invadopodial and peripheral glows of similar amplitude and kinetics were also reliably detected with the other biosensor PM-GCaMP6f (**Fig**.**S1B** and **S1C**), suggesting that low-level Orai1-overexpression caused by the expression of the biosensor GCaMP6f-Orail did not alter the properties of Ca^{2+} glows. More importantly, Ca^{2+} glows were better detected by the membrane-targeting biosensor than the diffusible cytosolic indicator Rhod4: in dual-indicator imaging experiments, Ca^{2+} glows reported by GCaMP6f-Orail were significantly brighter and had a higher signal-to-noise ratio (**Fig. S2B**); and small Ca^{2+} glows clearly visible with GCaMP6f-Orai1 were indiscernible with Rhod4 (**Fig. S2C**). Together with the *in situ* comparison of indicator properties shown in **Fig. S2A**, this result is consistent with the idea that invadopodial and peripheral glows originate mainly from Ca^{2+} influx rather than Ca^{2+} release.

Ca^{2+} Glows Represent Elemental Ca^{2+} Signals of SOCE

Next we sought to determine the specific link between specific Ca^{2+} sources and invadopodial or peripheral Ca^{2+} glows. We first demonstrated that removal of external Ca^{2+} led to a complete inhibition of Ca^{2+} glow activity (**Video 2**), indicating that Ca^{2+} influx as a prerequisite of Ca^{2+} glow production. Since we have previously shown that TRPM7 (a stretch-activated Ca^{2+}-permeant channel of the transient receptor potential superfamily) was able to generate discrete, though much briefer, local Ca^{2+} transients (Ca^{2+} flickers) in the leading lamellipodium of migrating fibroblasts. We investigated the role of TRPM7 in the generation of Ca^{2+} glows in WM793 cells. We showed that ablation of TRPM7 using CRISPR-Cas9 (**Fig. 3A**) had little effect on the frequency (**Fig. 3B** and **S3E**), amplitude (**Fig. 3C**), and kinetics of glows (**Fig. 3D**); neither did it significantly change the formation of invadopodia (**Fig. 3E**). Taken together, our data indicate that TRPM7 is unlikely to be the primary Ca^{2+} entry pathway in generating Ca^{2+} glows or in regulating invadopodial formation in WM793 cells.

In non-excitable cells, SOCE is activated by the depletion of the ER store and constitutes the major Ca^{2+} entry mechanism for refilling the internal store and sustaining cytoplasmic Ca^{2+} signaling. Recent reports have shown that STIM1-Orail-mediated SOCE occurs at discrete sites where STIM1 anchored in the ER and Orai1 in the plasma membrane form closely-apposed clusters in transfected cells. In testing whether Ca^{2+} glows reflect local, intermittent SOCE activity in native cells, we found that addition of 100 μM 2-APB, a commonly-used SOCE inhibitor, significantly suppressed the glow activity (**Fig. 4C** and **4D**) , consistent with the notion that glows depend on SOCE-related activity. Since 2-APB is not a very specific inhibitor, to directly test the SOCE hypothesis for the genesis of Ca^{2+} glows, we either expressed the dominant-negative Orai1 mutant, Orai1-E106A (**Fig. 4A**), or used CRISPR-Cas9 to knock out STIM1 in WM793 cells (**Fig. 4B**). Measurement of the cytosolic Ca^{2+} response using the Ca^{2+} indicator Fluo4 confirmed that, upon restoration of external Ca^{2+} after ER depletion, global SOCE was largely abolished by 2-APB, Orai1 E106A, or STIM1 knockout (KO) in WM793 cells (**Fig. 4C**). In these SOCE-abrogated cells, the occurrence of invadopodial and peripheral glows was dramatically suppressed by 87.7% and 67.4% in Orai1-E106A cells, and by 86.1% and 63.9% in STIM1-KO cells (**Fig. 4D** and **S3E**), strongly suggesting that Ca^{2+} glows originate from STIM1-Orai1-mediated local SOCE. Meanwhile, the formation of invadopodia was also significantly attenuated under the above conditions (**Fig. 4E**), confirming an important role for SOCE in invadopodial formation.

More direct evidence that local, intermittent SOCE underlies invadopodial and peripheral Ca^{2+} glows was obtained in experiments with the standard protocol of Ca^{2+} re-addition after store depletion. When ER depletion was induced by TG in the absence of external Ca^{2+}, Ca^{2+} glow activity was completely quiescent, as was the case with removal of external Ca^{2+} alone (**Video 2**). Strikingly, upon re-addition of extracellular Ca^{2+} (2 mM), bright Ca^{2+} glows discharged immediately and synchronously in all invadopodia, as well as at discrete peripheral sites (**Fig. 4F, Video 2**). In the continued presence of TG to prevent ER refilling, delayed Ca^{2+} glows occurred at a high rate, in an asynchronous manner, with latencies ranging from 10 s to 490 s. Compared to spontaneous Ca^{2+} glows in resting cells, these delayed evoked invadopodial glows had a much higher amplitude ($\Delta F/F_0$ = 2.27, N = 46 events), suggesting a higher STIM1-Orai1 channel open probability and/or the involvement of greater numbers of channels. The overall duration of the cluster activation, however, was unchanged because the FDHM of evoked Ca^{2+} glows (~9.44 s) was comparable to that of spontaneous glows. Repetitive activity of Ca^{2+} glows was also evident in the same invadopodia, indicative of STIM1-Orai1 clusters operating in a discrete and intermittent fashion. These evoked Ca^{2+} glows were effectively abrogated by the SOCE blocker 2-APB (**Fig. 4G**), the expression of Orai1 E106A (**Fig. 4H**), and the knockout of STIM1 (**Fig. 4I**). Taken together, we conclude that spontaneous and evoked Ca^{2+} glows originate from local, transient SOCE at the single invadopodium (and peripheral punctum) level. In other words, SOCE does not operate in a continuous mode; rather, it comprises spatiotemporally discrete elementary events in the form of Ca^{2+} glows in WM793 cells.

Similar SOCE Ca^{2+} glows were also found in human umbilical vein endothelial cells (HUVECs) (**Fig. S3F**), in which SOCE has been shown to actively participate in the regulation of proliferation and migration (Abdullaev Iskandar et al., 2008; Li et al., 2011). These Ca^{2+} glows were significantly inhibited by the SOCE blocker BTP-2 and the Orai1 dominant-negative mutant E106A (**Fig. S3G**). Thus, the conclusion that SOCE comprises discrete Ca^{2+} glows, akin to Ca^{2+} sparks and puffs for store Ca^{2+} release, might be generalizable to other non-excitable cells.

Ca^{2+}/calmodulin-dependent Pyk2 Activation by STIM1 and Orai1 in Invadopodial Formation

High-Ca^{2+} microdomains created by SOCE in the assembling invadopodium or invadopodial SOCE glows may spatially and temporally activate a multitude of local Ca^{2+}-dependent signaling cascades critical to cytoskeletal dynamics such as actin remodeling, focal adhesion detachment and relocation, and actin-myosin contraction (Wei et al., 2012). SOCE can regulate invadopodial initiation by activating non-receptor tyrosine kinase Src (Sun et al., 2014). Interestingly, the activation of Src by STIM1 was only found in adherent cells but not in suspended cells (**Fig. S4A**), suggesting a role for cell adhesion in SOCE-mediated Src activation. Pyk2 is a Ca^{2+}/calmodulin-dependent cell adhesion kinase (Riggs et al., 2011). The binding of Ca^{2+}/calmodulin to the autoinhibitory FERM domain leads to the formation of Pyk2 dimers (Kohno et al., 2008), and promotes the autophosphorylation and activation of Pyk2. To determine whether Pyk2 plays roles in SOCE-mediated invadopodial formation, we first investigated the effects of STIM1 and Orai1 on Pyk2 activity in WM793 cells. Depletion of STIM1 and Orai1 with shRNA reduced the levels of pY402-Pyk2 in WM793 cells by 50% and 80%, respectively (**Fig. 5A**). When ectopically expressed, STIM1 or STIM1 plus Orai1 increased

phospho-Pyk2 by more than 3-fold (**Fig. 5B**). Blockade of SOCE with 2-APB decreased phospho-Pyk2 by >80% (**Fig. 5C**), suggesting that SOCE is critical for Pyk2 activation.

To further test the hypothesis that SOCE activates Src through Pyk2, we used shRNA to knock down Pyk2, which resulted in a 70% reduction in Pyk2 protein levels (**Fig. 5D**). Overexpression of STIM1 in control shRNA-treated cells more than doubled the pY416-Src level; strikingly, the activation of Src by ectopic STIM1 was almost abrogated when Pyk2 was knocked down in WM793 cells (**Fig. 5D**), suggesting that Pyk2 is required for the SOCE-mediated activation of Src. Furthermore, the invadopodial formation and melanoma cell invasion promoted by SOCE were abolished after Pyk2 knockdown (**Fig. 5G** and **5H**).

To determine the mechanism by which SOCE activates Pyk2, we use W7 to inhibit calmodulin in WM793 cells expressing ectopic STIM1. W7 almost abolished the STIM1-induced Pyk2 autophosphorylation, suggesting that calmodulin is required for SOCE-mediated Pyk2 activation (**Fig. S4B**). It has been reported that 8–12 μM of free Ca^{2+} is required for the initial Pyk2 activation, although the activity of activated Pyk2 can be maintained in 500 nM free Ca^{2+} (Kohno et al., 2008). These results suggested that Pyk2 might serve as a downstream effector mediating the regulation of invadopodial formation by glows. Indeed, we noted that the active form of Pyk2 (pY402) and calmodulin were mostly localized to invadopodia and focal adhesions, implying that calmodulin and Pyk2 might be involved in modulating invadopodia and Src (**Fig. 5E** and **5F**). Moreover, Pyk2 was co-immunoprecipitated with calmodulin after 10% FBS induction initiated the growth of invadopodia, while they remained without interaction when cells were starved and quiescent (**Fig. S4C**). To further critically test this hypothesis, we generated a L176A/Q177A Pyk2 IQ motif mutant, which prevents the binding of calmodulin to the Pyk2 FERM domain (Kohno et al., 2008). Stimulation of Ca^{2+} influx with STIM1

overexpression remarkably increased the amount of Src co-immunoprecipitated by Pyk2, suggesting that SOCE promotes the physical interaction between Pyk2 and Src (**Fig. 5I**). However, when the Ca^{2+}/calmodulin-binding motif in the FERM domain of Pyk2 was mutated, this Pyk2-Src interaction was inhibited (**Fig. 5I**), indicating that the binding of calmodulin to the Pyk2 FERM domain is required for SOCE to regulate Src activity. Therefore, our data suggested that SOCE promotes invadopodial formation and melanoma invasion *via* the Ca^{2+}/calmodulin-Pyk2-Src pathway (**Fig. 5J**).

Discussion

In order to directly visualize the Ca^{2+} dynamics mediated by Orai1-STIM1 at high spatiotemporal resolution, we developed two types of Ca^{2+} biosensors, GCaMP6f-Orai1 and PM-GCaMP6f, and both were successfully targeted to the plasma membrane. This approach enabled us to visualize subsurface Ca^{2+} microdomains with high fidelity (as compared with the diffusible Ca^{2+} indicator Rhod4), while retaining sensitivity to Ca^{2+} changes in the bulk of the cytosol (through diffusion of Ca^{2+} into the subsurface). Our imaging data showed that Orai1 was locally and intermittently activated to mediate invadopodial and peripheral Ca^{2+} glows in invading WM793 cells as well as spatiotemporally discrete Ca^{2+} glows in HUVECs. We provided strong evidence that the Ca^{2+} glows in WM793 cells are elementary SOCE events, presumably mediated by the STIM1-Orai1 channel clusters. Unlike Ca^{2+} sparks of ryanodine receptor origin or Ca^{2+} puffs of IP_3R origin (Yao and Parker, 1994), the Ca^{2+} glows of SOCE origin were exceptionally long-lasting, and were blocked by removal of external Ca^{2+} and persisted under conditions that do not support any ER Ca^{2+} release (i.e., re-addition of external Ca^{2+} after store depletion in the continued presence of TG). SOCE Ca^{2+} glows are neither of the same nature as "Ca^{2+} flickers" (Wei et al., 2009) because their rate of occurrence was unaffected by TRPM7-

knockout as well as their distinctive kinetics. More importantly, inhibition of SOCE using pharmacological inhibitors, Orai1 dominant-negative mutant, or STIM1-knockout, effectively abolished Ca^{2+} glow activity. Upon restoration of external Ca^{2+} to cells with a depleted ER and disabled ER Ca^{2+} recycling, evoked STIM1-Orail Ca^{2+} glows occurred abruptly, followed by persistent discharge of high-rate, asynchronous Ca^{2+} glows. Using the plasma membrane-targeted biosensors G-GECO1-Orai1 and G-GECO1-Orai3 in conjunction with TIRF microscopy, Dynes et al. have previously visualized single Orai1 channel Ca^{2+} influx, artificially activated by co-expressing CAD or STIM1 or by 2-APB acting as an agonist of Orai3, in transfected cells (Dynes et al., 2016). However, the individual SOCE Ca^{2+} glows in the present study must each involve numerous Orai channels, given their spatial extent (up to 16 μm^2), large amplitude ($\Delta F/F_0$ up to 4-fold) and the small conductance of a single Orai channel. Thus, we have provided the first demonstration of elementary SOCE events originating from STIM1-Orail clusters in native cells under physiologically and pathologically relevant conditions.

The characterization of SOCE Ca^{2+} glows has uncovered surprising gating properties of STIM1 and Orai1 channel clusters *in situ*. First of all, the presence of discrete transient SOCE events indicates that SOCE operates in a digital, intermittent fashion, whereby store depletion markedly increases the rate of occurrence of Ca^{2+} glows with only modest changes of their unitary properties (i.e., amplitude and duration). Second, the presence of Ca^{2+} glow activity in resting cells shows that spontaneous SOCE activity is under tight spatial control such that adjacent invadopodia can exhibit distinctly different temporal patterns of activity. The high-Ca^{2+} microdomains so created by Ca^{2+} glows, coupled with local enrichment of Ca^{2+} effectors including calmodulin and Pyk2, might play a critical role in shaping the invadopodial dynamics as well as secretory functions for the initiation of invadopodial formation. Indeed, our data show

that the number of invadopodia in different experimental settings is closely related to the level of STIM1-Orail Ca^{2+} glow activity.

Based on the kinetics of Ca^{2+} glows, the gating of Orai1 channels within single invadopodia appear to be temporally synchronized and spatially coordinated. The rapid on- and off-kinetics of individual Ca^{2+} glows strongly argue against the hypothesis that individual Orai1 channels gate stochastically and independently. Possible mechanisms for the spatiotemporal coordination of Orai1 channels at the invadopodial level could be twofold. If the ER store fluctuates locally, then the Orai1 channels in the same invadopodium may share a common modulatory signal so they operate in concert. However, invadopodial and peripheral Ca^{2+} glows occur in ER-depleted cells with disabled Ca^{2+} recycling, indicating that this could not be the sole explanation. Alternatively, a single STIM-Orai channel may act as an intrinsic oscillator and manifest dampened oscillatory behavior under certain experimental conditions (Dynes et al., 2016). In this scenario, an entrained oscillation of many STIM1-Orai1 channels in the same invadopodium (punctum) would afford a possible explanation for the invadopodium (punctum)-level synchrony.

Local control of Ca^{2+} signaling is essential for this vital intracellular messenger to control diverse physiological and pathophysiological processes (Berridge et al., 2000). The activation of low-affinity Ca^{2+}-binding proteins requires tens to hundreds of micromoles of Ca^{2+}, which is orders of magnitude higher than the physiological Ca^{2+} concentration in the bulk of the cytosol. With a 10^4-fold Ca^{2+} gradient built up across the plasma membrane, SOCE, which is prevalent in most cell types, comprises the major Ca^{2+} entry pathway. It has been estimated that in the microdomain within the opening mouth of activated SOC channels, the Ca^{2+} concentration can reach tens of micromoles (Hogan, 2015; Kar et al., 2014), a concentration sufficient to activate

many Ca^{2+} effectors with low Ca^{2+}-binding affinity. In this study, we found that calmodulin and Pyk2 are enriched in invadopodia and co-exist with intermittent high-Ca^{2+} signals in the form of Ca^{2+} glows. In this regard, previous studies have provided evidence that the NFAT1 transcription factor and adenylyl cyclase 8 are selectively activated by SOC-mediated subplasmalemmal Ca^{2+} microdomains, but not by a global increase in cytosolic Ca^{2+} (Kar et al., 2011; Willoughby et al., 2012). In this case, invadopodia and podosomes are proteolytic membrane protrusions used by invasive cells to remodel the extracellular matrix. It has been demonstrated that Ca^{2+} channels and effectors such as Orai1, STIM1, myosin, and calcineurin are enriched in invadopodia and podosomes (Alexander et al., 2008; Baldassarre et al., 2003; Chen et al., 2017; Siddiqui et al., 2012). Interestingly, calmodulin and the Ca^{2+}-activated adhesion kinase Pyk2 are also locally recruited to invadopodia. By recruiting SOC channels and Ca^{2+} effectors, invadopodia may serve as signaling hubs (Mo and Yang, 2018), coordinating invadopodial initiation and extracellular matrix degradation through a Ca^{2+}/calmodulin-Pyk2-Src pathway.

In summary, we have investigated the spatiotemporal dynamics of SOCE using orai1-tethered or palmitoylated Ca^{2+} biosensors in conjunction with confocal microscopy. We discovered elementary SOCE events, namely Ca^{2+} glows, in invading cancer cells as well as primary cultured endothelial cells. Using Ca^{2+} glows as optical recordings of the activation and Ca^{2+} permeation of STIM1-Orai1 channel clusters, we revealed unexpected gating properties and their regulation of these SOC channels *in situ*. Functionally, intermittent invadopodial Ca^{2+} glows may play an essential role in the activation of locally enriched, high-threshold Ca^{2+} effectors required for invadopodial formation and cancer metastasis. Future investigations are warranted to determine to what extent the current findings can be generalized to other types of

non-excitable cells and how the spatiotemporal organization of elemental SOCE events can orchestrate complex cell behaviors in physiology and pathology.

Materials and Methods

Vector construction and recombinant adenovirus production

The GCaMP6f and human Orai1 genes were amplified from pGP-CMV-GCaMP6f (Addgene #40755) and Orai1-EGFP (Yang et al., 2009), respectively, and then inserted into pEGFP-C1 *via* an in-fusion cloning kit (Clontech). The Orai1 dominant-negative mutant Orai1-E106A was amplified from myc-Orai1 E106A pHAGE (Addgene #22752). For PM tethering, the GCaMP6f sequence was inserted into the BamHI and NotI restriction sites of PM-FRB-CFP (Addgene #67517) through ligation. The fusion gene GCaMP6f-Orai1, the Orai1-E106A mutant, and PM-GCaMP6f were then amplified and inserted into the pENTR/TEV/D-TOPO vector (Invitrogen). The adenovirus was produced in HEK293A cells using an adenoviral expression system (Invitrogen).

Cell culture

The culture media used for WM793 melanoma cells were RPMI (Gibco) and DMEM (Gibco) for HEK293A and HEK293T cells. All culture media were supplemented with 10% FBS and penicillin/streptomycin.

RNA interference

RNA interference of STIM1, Orai1, and Pyk2 was performed using the pSUPER.Retro.puro vector (Oligoengine) encoding small-hairpin RNA. The target sequences were as following: AGAAGGAGCTAGAATCTCAC (STIM1sh), TCGGCCTGATCTTTATCGT (Orai1sh1), CCAGCATTGAGTGTGTACA (Orai1sh2), TGCACTTGACAAGAAGTCC (Pyk2sh1), and ACCCAGAAACTGCTCAACA (Pyk2sh2). To efficiently knock down Orai1 and Pyk2, two shRNAs targeting two different regions of the same gene were used simultaneously. Cells with stable knock-down were selected using 2 μg/mL puromycin.

CRISPR-Cas9 gene knockout system

The targeting guide sgRNAs were cloned into the BsmBI restriction site of the pLentiCRISPRv2 backbone vector (Addgene #52961). The sequences were GGCGACAGGAACCAGCTCGG for STIM1, and TGACTCCATAAGCATCCGTT for TRPM7.

Stable cell line construction

Stable cell lines were generated *via* the pLPCX and pLNCX2 retroviral systems. The pLNCX2 retroviral vectors encoding human STIM1 have been previously described (Yang et al., 2012). pLPCX-Flag-Pyk2 was generated by cloning Flag-Pyk2 into pLPCX between the BglII and XhoI restriction sites. The Flag-Pyk2 FERM domain mutation (Pyk2 L176A/Q177A) was generated by direct mutagenesis using pLPCX-Flag-Pyk2 as template, with the forward primer, 5'-CTGGGCCACTACGCGGAGCGGAACAAGAACTCCGCGAAGGCGCTCACCCTCGCGCT GTACTCACTG-3', and the reverse primer, 5'-CAGTGAGTACAGCGCGAGGGTGAGCGCCTTCGCGGAGTTCTTGTTCCGCTCCGCGTA GTGGCCCAG-3'. The vectors were then transfected into HEK293T cells along with VSV-G

and gag-pol to generate mature retrovirus. Positive stable cells were selected using G418 (400 µg/mL) for pLNCX2 and puromycin (2 µg/mL) for pLPCX.

Western blotting analysis

Cell lysates were separated by 4–12% SDS-PAGE and transferred to nitrocellulose membranes (Millipore). The membranes were blocked with 5% non-fat dry milk and incubated with primary antibody overnight at 4°C, followed by incubation with secondary antibodies for 1 h at room temperature. Antibodies to STIM1 (Cell Signaling #5668S), Orai1 (Sigma-Aldrich #O8264), GAPDH (Sigma-Aldrich #G8795), Src (Millipore, clone GD11 #05-184), p-Src (Tyr416) (Cell Signaling #2101), Pyk2 (Cell Signaling #3480), p-Pyk2 (Tyr402) (Cell Signaling #3291), tubulin (Sigma-Aldrich #T6199), calmodulin (Santa Cruz Biotechnology #sc-137079), and TRPM7 (Abcam #109438) were used.

Immunofluorescence assay

WM793 cells were permeabilized with 0.1% Triton X-100 and blocked with 10% normal goat serum. The sections were incubated with rabbit anti-phospho-Pyk2 (Cell Signaling #3291) or mouse anti-calmodulin (Santa Cruz Biotechnology #sc-137079), both at 1:100 dilution, for 2 h at room temperature, washed with PBS, and then incubated with Alexa Fluor 488-conjugated anti-mouse IgG (1:300, Invitrogen) or anti-rabbit IgG (1:300, Invitrogen) and TRITC-labeled phalloidin (5 µg/mL, Sigma) for 1 h at room temperature. The immunofluorescence staining was visualized using a Zeiss LSM710 confocal microscope at 488 nm and 543 nm excitation and 490-550 and >560 nm emission, respectively.

Co-immunoprecipitation assay

WM793 cells expressing pLPCX control and pLPCX-Flag-Pyk2 grown to 90% confluence were washed three times with ice-cold PBS and lysed in 0.5 mL lysis buffer (50 mM Tris, 150 mM NaCl, 0.5% sodium deoxycholate, 1% Triton X-100, pH 8.0). The cell lysate was briefly sonicated (5 s) and centrifuged at 14,000 rpm on a 4°C benchtop centrifuge. The supernatant was incubated with M2 beads for 4 h at 4°C, then the beads were washed three times with wash buffer (50 mM Tris, 150 mM NaCl, 1 mM PMSF, and 1% NP-40, pH 8.0) and the bound proteins were eluted with protein sample buffer, resolved on SDS-PAGE, and detected with calmodulin or Src antibody.

Fluorescent gelatin labeling

Fluorescent gelatin was synthesized by incubating bovine skin gelatin with amine-reactive fluorescent dyes. TRITC isothiocyanate (Thermo) was dissolved in DMSO at 10 mg/mL. Dye solution (50 µL) was added slowly to 1 mL of bovine skin gelatin solution (Sigma) (40 mg/mL, dissolved in 0.1 M sodium bicarbonate buffer, pH 8.3) while vortexing. After incubation at room temperature for 1 h, the free dyes in the mixture were removed with a HiTrap desalting column (GE Life Sciences). The desalted fluorescent gelatin solution can be stored at 4°C for short-term storage or at -80°C with 10% glycerol as cryoprotectant for long-term storage.

Coverslip coating

Acid-washed coverslips (or glass-bottomed dishes) were incubated with 0.4% bovine gelatin for 30-60 min and washed with PBS. The gelatin was fixed with 0.5% glutaraldehyde for 10 min and then washed extensively with PBS for cell culture and imaging.

Live cell imaging

WM793 cells (in RPMI growth medium with 10% FBS) were plated onto gelatin-coated coverslips or glass-bottomed dishes to attach and spread for at least 3 h and then starved overnight (>12 h) in RPMI with 1% FBS. Invadopodial formation was initiated by adding 10% FBS to the starvation medium.

Confocal imaging was carried out with a Zeiss LSM710 microscope with a 40×, 1.3 N.A. oil-immersion objective; the pinhole was set for a nominal 1-µm optical section. Cells were kept in a Heating Insert P S1 incubator (Pecon) at a constant temperature of 37 °C under 5% CO_2 (vol/vol). For simultaneous measurement of GCaMP6f-Orai1 or Fluo4 and Lifeact-mApple or Rhod4, excitation was at 488 and 543 nm and their fluorescence emission was collected at 490-520 (with Rhod4) or 490-540 (with Lifeact-mApple) and >560 nm, respectively. For chemical Ca^{2+} indicator loading, WM793 cells were incubated with 5 µmol/L Rhod4 AM (AAT Bioquest) or Fluo4 AM (Invitrogen) for 10 min at 37 °C. Linescan imaging was performed at 3.78 ms/line and x-y time-lapse images were acquired at 0.78 s/frame every 5 s.

Image processing and data analysis

Digital images were processed using customer-devised routines written in IDL (ITT, New York, NY). Data are reported as the mean ± SEM. Two-tailed p values were determined by Student's t-test or the Mann-Whitney test as indicated, with $p < 0.05$ defined as statistically significant.

Acknowledgements

We thank Dr. Iain C. Bruce for manuscript editing, Dr. Shiqiang Wang, Chaoliang Wei, and Kunfu Ouyang for valuable comments, and Dr. Yujie Sun, Dong Li, and Liangyi Chen for assistance with imaging experiments.

Competing interests

The authors declare no potential conflicts of interest.

Funding

This work was supported by the National Key R&D Program of China (2017YFA0504000 and 2016YFA0500403 to H. Cheng) and the National Natural Science Foundation of China (31470811, 31670039, and 31521062 to H. Cheng; 31671448 and 81572618 to J. Sun) and the National Institutes of Health (R01CA175741 to S. Yang).

Author contributions

F.L., J.S., S.Y. and H.C. conceived and designed the study. F.L. and C.H. developed the methodology for Ca^{2+} imaging. F.L. and J.S. conducted most of the experiments, and analyzed and interpreted the data. Q.Z., J.L., Y.H., P.Y., H.H., Y.Z., and X.W. helped with part of data collection and figure preparation. F.L., S.Y., and H.C. wrote the manuscript.

References

Abdullaev Iskandar, F., Bisaillon Jonathan, M., Potier, M., Gonzalez Jose, C., Motiani Rajender, K. and Trebak, M. (2008). Stim1 and Orai1 Mediate CRAC Currents and Store-Operated Calcium Entry Important for Endothelial Cell Proliferation. *Circulation Research* **103**, 1289-1299.

Alexander, N. R., Branch, K. M., Parekh, A., Clark, E. S., Iwueke, I. C., Guelcher, S. A. and Weaver, A. M. (2008). Extracellular matrix rigidity promotes invadopodia activity. *Curr. Biol.* **18**, 1295-9.

Baldassarre, M., Pompeo, A., Beznoussenko, G., Castaldi, C., Cortellino, S., McNiven, M. A., Luini, A. and Buccione, R. (2003). Dynamin participates in focal extracellular matrix degradation by invasive cells. *Mol. Biol. Cell.* **14**, 1074-84.

Berridge, M. J., Bootman, M. D. and Roderick, H. L. (2003). Calcium signalling: dynamics, homeostasis and remodelling. *Nat. Rev. Mol. Cell Biol.* **4**, 517-29.

Berridge, M. J., Lipp, P. and Bootman, M. D. (2000). The versatility and universality of calcium signalling. *Nat. Rev. Mol. Cell Biol.* **1**, 11-21.

Chen, J. and Sanderson, M. J. (2017). Store-operated calcium entry is required for sustained contraction and Ca2+ oscillations of airway smooth muscle. *The Journal of Physiology* **595**, 3203-3218.

Chen, T. W., Wardill, T. J., Sun, Y., Pulver, S. R., Renninger, S. L., Baohan, A., Schreiter, E. R., Kerr, R. A., Orger, M. B., Jayaraman, V. et al. (2013). Ultrasensitive fluorescent proteins for imaging neuronal activity. *Nature* **499**, 295-300.

Chen, Y. W., Chen, Y. F., Chiu, W. T., Chen, H. C. and Shen, M. R. (2017). STIM1-dependent Ca(2+) signaling regulates podosome formation to facilitate cancer cell invasion. *Sci. Rep.* **7**, 11523.

Cheng, H., Lederer, W. and Cannell, M. (1993). Calcium sparks: elementary events underlying excitation-contraction coupling in heart muscle. *Science* **262**, 740-744.

Cheng, H. and Lederer, W. J. (2008). Calcium sparks. *Physiol. Rev.* **88**, 1491-545.

Dynes, J. L., Amcheslavsky, A. and Cahalan, M. D. (2016). Genetically targeted single-channel optical recording reveals multiple Orai1 gating states and oscillations in calcium influx. *Proc. Natl. Acad. Sci. USA.* **113**, 440-445.

Feldman, C. H., Grotegut, C. A. and Rosenberg, P. B. (2017). The role of STIM1 and SOCE in smooth muscle contractility. *Cell Calcium* **63**, 60-65.

Gimona, M., Buccione, R., Courtneidge, S. A. and Linder, S. (2008). Assembly and biological role of podosomes and invadopodia. *Curr. Opin. Cell Biol.* **20**, 235-41.

Hogan, P. G. (2015). The STIM1-ORAI1 microdomain. *Cell Calcium* **58**, 357-67.

Kar, P., Nelson, C. and Parekh, A. B. (2011). Selective activation of the transcription factor NFAT1 by calcium microdomains near Ca(2+) release-activated Ca(2+) (CRAC) channels. *J. Biol. Chem.* **286**, 14795-803.

Kar, P., Samanta, K., Kramer, H., Morris, O., Bakowski, D. and Parekh, A. B. (2014). Dynamic assembly of a membrane signaling complex enables selective activation of NFAT by Orai1. *Curr. Biol.* **24**, 1361-1368.

Kohno, T., Matsuda, E., Sasaki, H. and Sasaki, T. (2008). Protein-tyrosine kinase CAKbeta/PYK2 is activated by binding Ca(2+)/calmodulin to FERM F2 alpha2 helix and thus forming its dimer. *Biochem. J.* **410**, 513-23.

Li, J., Cubbon Richard, M., Wilson Lesley, A., Amer Mohamed, S., McKeown, L., Hou, B., Majeed, Y., Tumova, S., Seymour Victoria, A. L., Taylor, H. et al. (2011). Orai1 and CRAC Channel Dependence of VEGF-Activated Ca2+ Entry and Endothelial Tube Formation. *Circulation Research* **108**, 1190-1198.

Li, Z., Lu, J., Xu, P., Xie, X., Chen, L. and Xu, T. (2007). Mapping the interacting domains of STIM1 and Orai1 in Ca(2+) release-activated Ca(2+) channel activation. *J. Biol. Chem.* **282**, 29448-56.

Linder, S. (2007). The matrix corroded: podosomes and invadopodia in extracellular matrix degradation. *Trends Cell Biol.* **17**, 107-17.

Liou, J., Kim, M. L., Heo, W. D., Jones, J. T., Myers, J. W., Ferrell, J. E., Jr. and Meyer, T. (2005). STIM is a Ca(2+) sensor essential for Ca(2+)-store-depletion-triggered Ca(2+) influx. *Curr. Biol.* **15**, 1235-41.

Mo, P. and Yang, S. (2018). The store-operated calcium channels in cancer metastasis: from cell migration, invasion to metastatic colonization. *Front. Biosci.* **23**, 1241-1256.

Murphy, D. A. and Courtneidge, S. A. (2011). The 'ins' and 'outs' of podosomes and invadopodia: characteristics, formation and function. *Nat. Rev. Mol. Cell Biol.* **12**, 413-26.

Parekh, A. B. and Putney, J. W., Jr. (2005). Store-operated calcium channels. *Physiol. Rev.* **85**, 757-810.

Park, C. Y., Hoover, P. J., Mullins, F. M., Bachhawat, P., Covington, E. D., Raunser, S., Walz, T., Garcia, K. C., Dolmetsch, R. E. and Lewis, R. S. (2009). STIM1 clusters and activates CRAC channels via direct binding of a cytosolic domain to Orai1. *Cell* **136**, 876-90.

Prakriya, M. and Lewis, R. S. (2015). Store-operated calcium channels. *Physiol. Rev.* **95**, 1383-436.

Riggs, D., Yang, Z., Kloss, J. and Loftus, J. C. (2011). The Pyk2 FERM regulates Pyk2 complex formation and phosphorylation. *Cell. Signal.* **23**, 288-96.

Samanta, K., Kar, P., Mirams, G. R. and Parekh, A. B. (2015). Ca(2+) channel re-localization to plasma-membrane microdomains strengthens activation of Ca(2+)-dependent nuclear gene expression. *Cell Rep.* **12**, 203-16.

Shang, W., Lu, F., Sun, T., Xu, J., Li, L. L., Wang, Y., Wang, G., Chen, L., Wang, X., Cannell, M. B. et al. (2014). Imaging Ca(2+) nanosparks in heart with a new targeted biosensor. *Circ. Res.* **114**, 412-20.

Siddiqui, T. A., Lively, S., Vincent, C. and Schlichter, L. C. (2012). Regulation of podosome formation, microglial migration and invasion by Ca(2+)-signaling molecules expressed in podosomes. *J. Neuroinflammation* **9**, 250.

Smith, I. F., Wiltgen, S. M. and Parker, I. (2009). Localization of puff sites adjacent to the plasma membrane: Functional and spatial characterization of Ca(2+) signaling in SH-SY5Y cells utilizing membrane-permeant caged IP3. *Cell Calcium* **45**, 65-76.

Sun, J., Lu, F., He, H., Shen, J., Messina, J., Mathew, R., Wang, D., Sarnaik, A. A., Chang, W. C., Kim, M. et al. (2014). STIM1- and Orai1-mediated Ca(2+) oscillation orchestrates invadopodium formation and melanoma invasion. *J. Cell Biol.* **207**, 535-48.

Varnai, P., Thyagarajan, B., Rohacs, T. and Balla, T. (2006). Rapidly inducible changes in phosphatidylinositol 4,5-bisphosphate levels influence multiple regulatory functions of the lipid in intact living cells. *J. Cell Biol.* **175**, 377-82.

Wei-LaPierre, L., Carrell, E. M., Boncompagni, S., Protasi, F. and Dirksen, R. T. (2013). Orai1-dependent calcium entry promotes skeletal muscle growth and limits fatigue. *Nature Communications* **4**, 2805.

Wei, C., Wang, X., Chen, M., Ouyang, K., Song, L. S. and Cheng, H. (2009). Calcium flickers steer cell migration. *Nature* **457**, 901-5.

Wei, C., Wang, X., Zheng, M. and Cheng, H. (2012). Calcium gradients underlying cell migration. *Current Opinion in Cell Biology* **24**, 254-261.

Willoughby, D., Everett, K. L., Halls, M. L., Pacheco, J., Skroblin, P., Vaca, L., Klussmann, E. and Cooper, D. M. (2012). Direct binding between Orai1 and AC8 mediates dynamic interplay between Ca(2+) and cAMP signaling. *Sci. Signal.* **5**, ra29.

Wu, M. M., Buchanan, J., Luik, R. M. and Lewis, R. S. (2006). Ca(2+) store depletion causes STIM1 to accumulate in ER regions closely associated with the plasma membrane. *J. Cell Biol.* **174**, 803-13.

Yang, S., Zhang, J. J. and Huang, X. Y. (2009). Orai1 and STIM1 are critical for breast tumor cell migration and metastasis. *Cancer Cell* **15**, 124-34.

Yang, S., Zhang, J. J. and Huang, X. Y. (2012). Mouse models for tumor metastasis. *Methods Mol. Biol.* **928**, 221-8.

Yao, Y. and Parker, I. (1994). Ca(2+) influx modulation of temporal and spatial patterns of inositol trisphosphate-mediated Ca(2+) liberation in Xenopus oocytes. *J. Physiol.* **476**, 17-28.

Zhou, Y., Cai, X., Loktionova, N. A., Wang, X., Nwokonko, R. M., Wang, X., Wang, Y., Rothberg, B. S., Trebak, M. and Gill, D. L. (2016). The STIM1-binding site nexus remotely controls Orai1 channel gating. *Nat. Commun.* **7**, 13725.

Figures

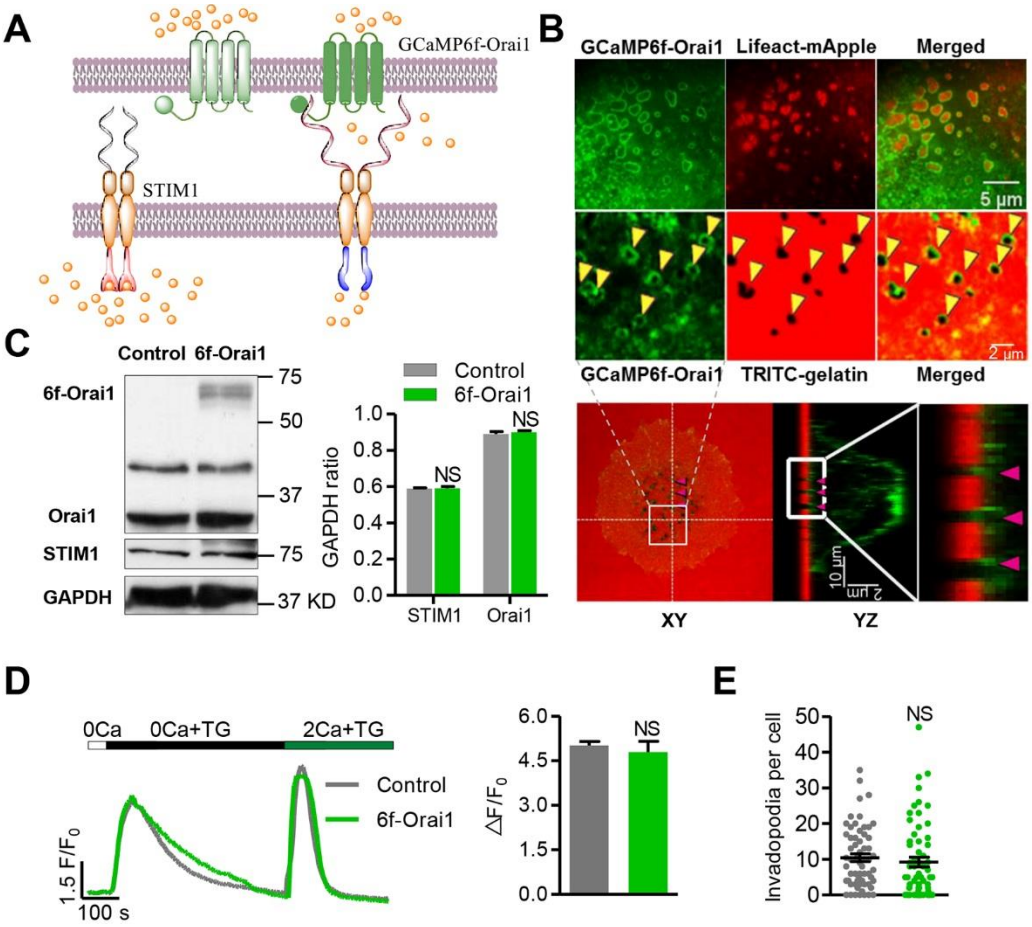

Fig. 1. Targeting the Ca^{2+} Biosensor GCaMP6f to the Plasma Membrane.

A, Schematic showing the design strategy of the GCaMP6f-Orai1 Ca^{2+} biosensor. GCaMP6f was fused to the N-terminus of Orai1 (GCaMP6f-Orai1) to target it to the plasma membrane with preferential accessibility to Orai1-meditated Ca^{2+} entry. This vector was expressed in WM793 cells by adenoviral infection. **B**, Localization of GCaMP6f-Orai1. From left to right, confocal images of GCaMP6f-Orai1, invadopodia visualized by Lifeact-mApple fluorescence (top) or degradation holes left (arrowheads) after TRITC-labeled gelatin was digested (middle, enlarged

view of the cell area indicated in the bottom panel), and their merged images. Note that the GCaMP6f-Orai1 fluorescence encircles invadopodia. Bottom, orthogonal views of confocal z stacks showing the localization of the targeted sensor, XY view (left), YZ view (middle) and enlarged view of the area indicated in the middle panel (right). **C**, Western blots showing the expression of GCaMP6f-Orai1 and its effect on endogenous STIM1 and Orai1 levels and its quantification. **D**, Effects of biosensor expression on thapsigargin (TG)-induced SOCE. Left, after store Ca^{2+} release induced by 5 μM TG in 0 Ca^{2+} solution; reintroducing Ca^{2+} into the extracellular solution elicited SOCE. Note that Rhod4 reported similar release and SOCE-induced cytosolic Ca^{2+} responses in control and GCaMP6f-Orai1-expressing cells. Right, statistics of the magnitude of SOCE, indexed by $\Delta F/F_0$ of Rhod4 after Ca^{2+} restoration following store depletion. n = 172 and 49 cells from 7 independent experiments for control and GCaMP6f-Orai1 groups, respectively. **E**, The number of invadopodia per cell was unaltered by the biosensor expression. n = 62 cells from 4 independent experiments for both groups. Data represent mean ± SEM. NS, not statistically significant.

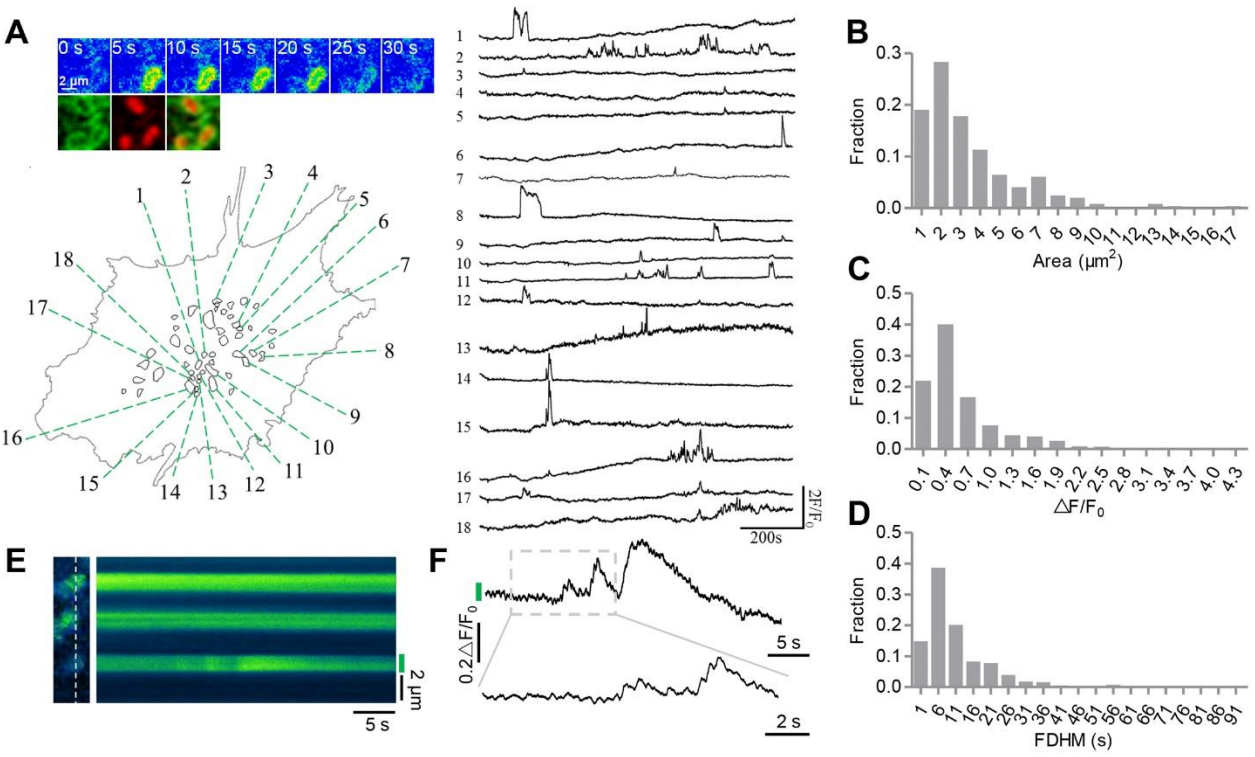

Fig. 2. Spontaneous invadopodial Ca^{2+} glows detected by GCaMP6f-Orai1.

A, Spontaneous invadopodial Ca^{2+} glows from a WM793 cell expressing GCaMP6f-Orai1. WM793 cells were infected with GCaMP6f-Orai1 adenovirus and plated on gelatin-coated coverslips. After starvation overnight, they were exposed to 10% FBS for 20 min to initiate the formation of invadopodia and then subjected to imaging. Individual invadopodia are outlined and numerically labeled. Upper left panels, time-lapse F/F_0 images at 5-s intervals of a representative invadopodial Ca^{2+} glow (first row) and local staining of GCaMP6f-Orai1 and Lifeact-mApple as well as the merged image (second row). Right panels, time courses of invadopodial Ca^{2+} glows. Note that the occurrence of Ca^{2+} glows appears to be independently regulated, even among adjacent invadopodia. See also **Video 1**. **B**, **C**, and **D**, Distributions of the area (**B**), amplitude (**C**), and duration (FDHM) (**D**) of invadopodial Ca^{2+} glows (n = 566 events from 36 cells in 30 independent experiments). **E**, High-resolution imaging of invadopodial Ca^{2+} signals. Inset:

dashed line across three adjacent invadopodia denotes the selected line for imaging at 3.78 ms/line. **F**, Time courses of GCaMP6f-Orai1 fluorescence corresponding to the image part marked by the green line in **E** are shown in parallel with the image and an expanded view of the boxed time window is shown below.

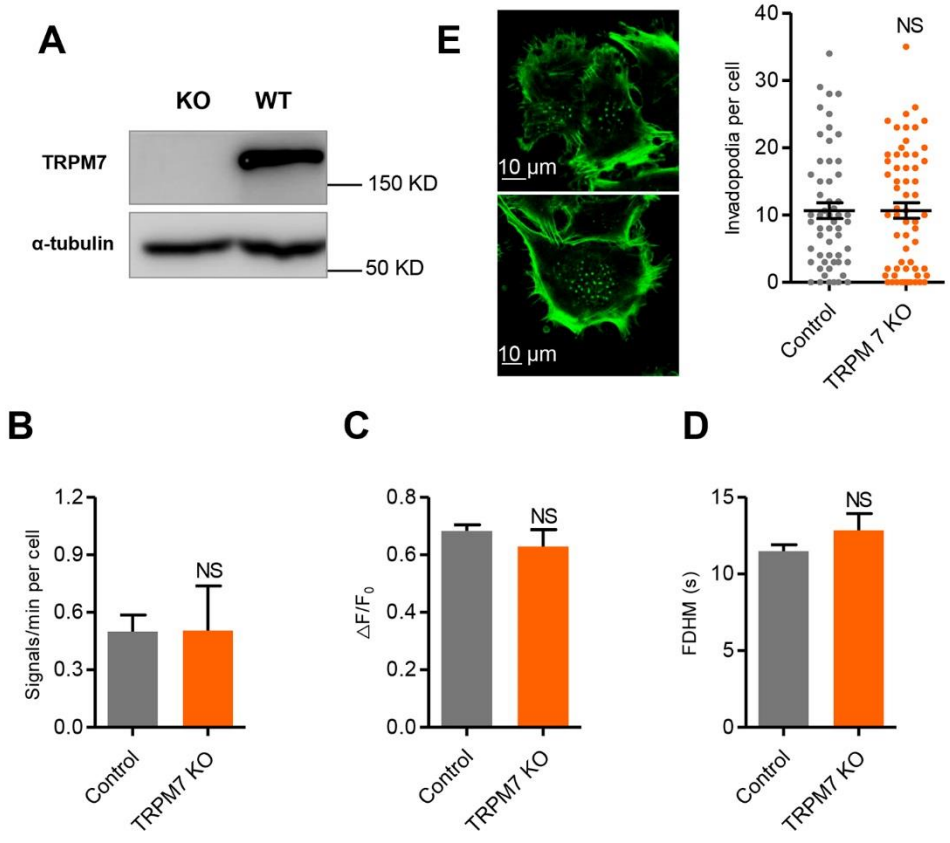

Fig. 3. TRPM7 is not responsible for the genesis of Ca^{2+} glows.

A, Western blots showing knockout of TRPM7. **B**, **C**, and **D**, Negligible effects of TRPM7 KO on the frequency (**B**), amplitude ($\Delta F/F_0$) (**C**), and duration (FDHM) (**D**) of invadopodial Ca^{2+} glows (n= 54 and 15 cells from 30 and 12 independent experiments for the control and TRPM7 KO groups, respectively). **E**, Left panel, fluorescence micrographs showing invadopodial formation in control and TRPM7 knockout (KO) cells. Right panel, quantification of invadopodial formation (n = 56 and 61 cells from 4 independent experiments for the control and TRPM7 KO groups). Data are presented as means ± SEM. NS, not statistically significant.

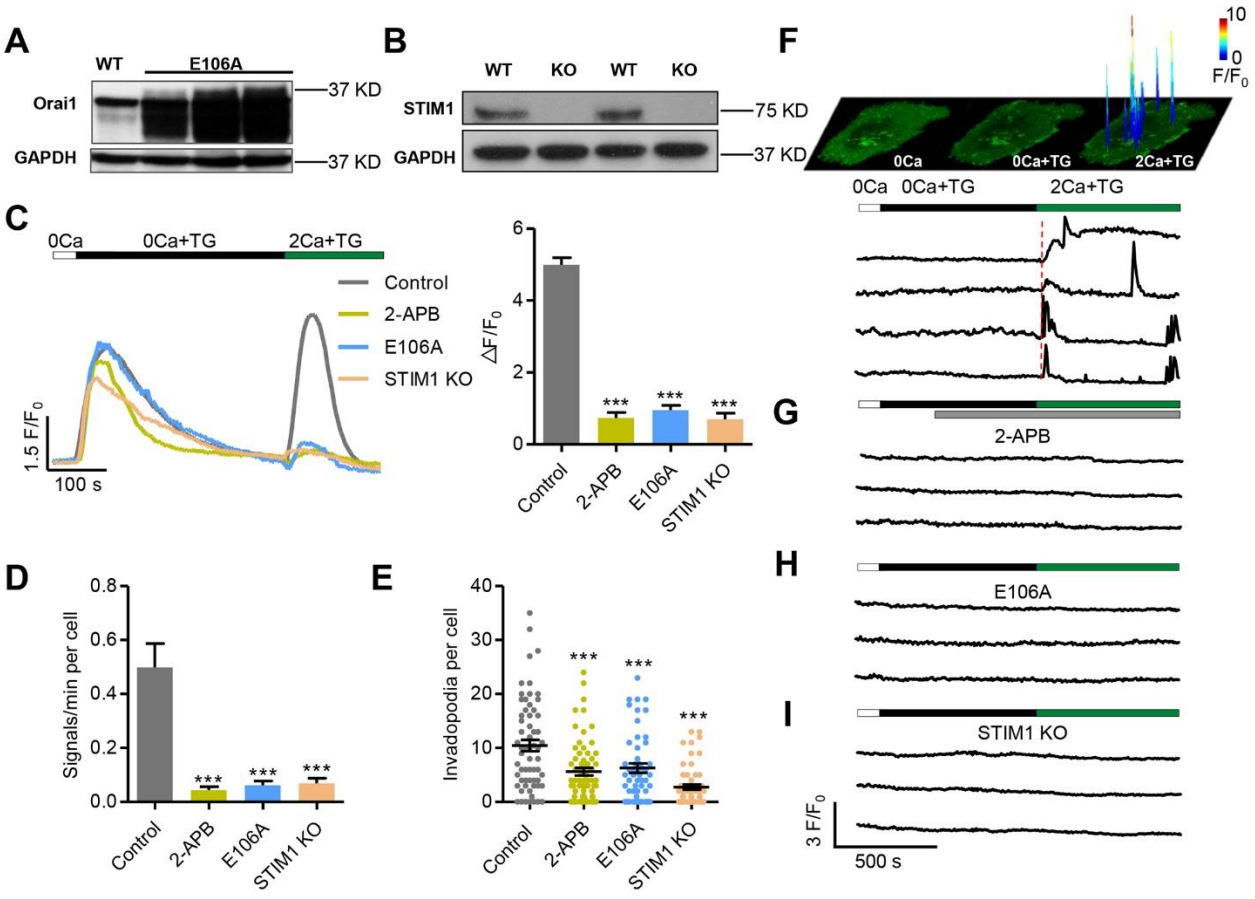

Fig. 4. Invadopodial Ca^{2+} glows originate from SOCE mediated by Orai1 and STIM1.

A and **B**, Manipulating SOCE in WM793 cells. Western blots showing the expression of the dominant-negative mutant Orai1-E106A (E106A) (**A**) and knockout of STIM1 (STIM1 KO) (**B**). **C**, Representative traces (left) and average amplitude (right) of SOCE recorded by Fluo4. 100 μM 2-APB was added to the extracellular solution when the fluorescence returned to baseline after TG treatment. Note that ER Ca^{2+} release was largely comparable in these groups (n = 69, 32, 61, and 83 cells from 3, 3, 9, and 3 independent experiments for control, 2-APB, E106A, and STIM1 KO groups, respectively). **D**, Statistics of the frequencies of spontaneous invadopodial Ca^{2+} glows (n = 54, 18, 21, and 36 cells from 30, 8, 16, and 25 independent experiments for control, 2-APB, E106A mutant, and STIM1 KO groups, respectively). **E**, Depression of

invadopodial formation by treatment with 2-APB (n = 66), expression of the E106A mutant (n = 52), and STIM1 KO (n = 57) compared to control (n = 62) from 6 independent experiments. **F**, Invadopodial Ca^{2+} glows resolved during global SOCE. Upper panel, space-time plots of local Ca^{2+} events reported by GCaMP6f-Orai1 in response to 0 Ca, TG, and subsequent 2 mM Ca^{2+} in a WM793 cell. The colored peaks are overlays of surface plots of discrete Ca^{2+} glows at their peaks, indicating both the locations and the amplitudes (coded by colors) of these local signals. Lower panel, corresponding traces of representative invadopodial Ca^{2+} glows during global SOCE. Note the initial near-synchronous activation at all invadopodia followed by delayed, asynchronous activity at individual invadopodia. **G**, **H**, and **I**, Invadopodial Ca^{2+} glows were abolished by 2-APB treatment (**G**), expression of the E106A mutant (**H**), and STIM1 KO (**I**). Data are presented as mean ± SEM; ***p <0.001 compared to control.

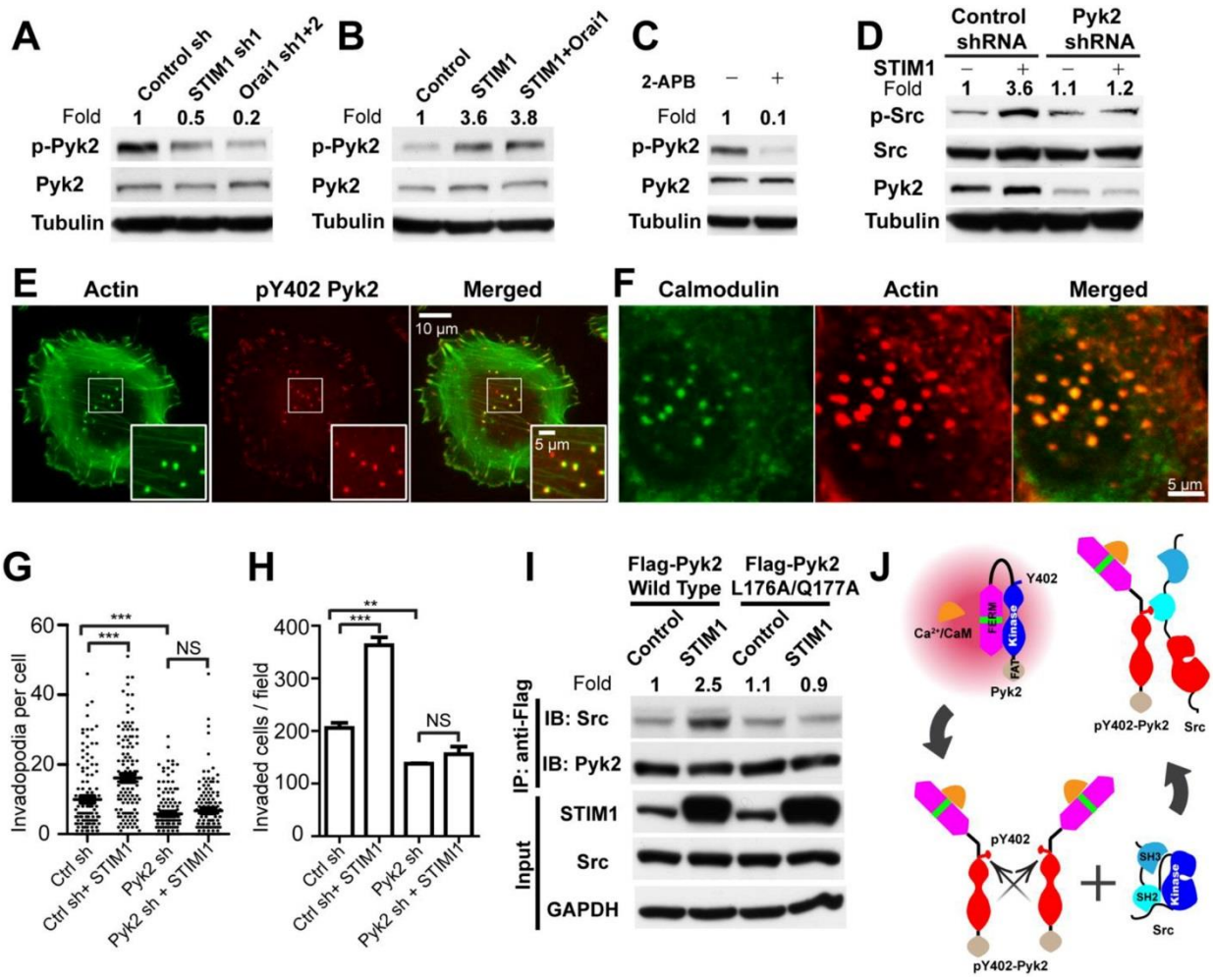

Fig. 5. SOCE regulates invadopodial formation through the Ca^{2+}/calmodulin-Pyk2-Src pathway.

A, STIM1 shRNA and Orai1 shRNA decreased active Pyk2 (pY402-Pyk2) levels in WM793 cells. **B**, Ectopic expression of STIM1 and Orai1 activated Pyk2 in WM793 cells. **C**, SOCE blockade with 2-APB (100 μM) decreased pY402-Pyk2 levels. **D**, Depletion of Pyk2 with shRNA abrogated the STIM1-mediated activation of pY416 -Src. **E**, Immunofluorescence staining of pY402-Pyk2 showing that Pyk2 was activated in invadopodia and focal adhesions in WM793 cells. **F**, Immunofluorescence staining showing that calmodulin was recruited to invadopodia in WM793 cells. **G**, Pyk2 knockdown abolished STIM1-mediated invadopodial

formation (n = 120, 123, 125, and 127 for control shRNA, control shRNA + STIM1, Pyk2 shRNA, and Pyk2 shRNA + STIM1, respectively). **H**, STIM1-promoted WM793 cell invasion was abrogated after Pyk2 knockdown. Cell numbers were collected from triplicate independent invasion chamber assays. **I**, Ectopic overexpression of STIM1 stimulated the interaction of Src with wild-type Pyk2, but not the calmodulin binding motif mutant of Pyk2 (L176Q/Q177A). **J**, A model for the Ca^{2+}/calmodulin-Pyk2-Src pathway downstream of SOCE. Local high Ca^{2+} influx mediated by SOCE promotes the binding of Ca^{2+}/calmodulin to the FERM domain of Pyk2, which releases the intra-molecular auto-inhibition. Ca^{2+}/calmodulin-bound Pyk2 autophosphorylate each other on tyrosine 402. pY402-Pyk2 interacts with the SH2 domain of Src to activate Src. Data are representative results from at least 3 independent experiments. Horizontal bars represent mean ± SEM; ***p <0.001, **p <0.01, NS, not statistically significant.

Fig. S1

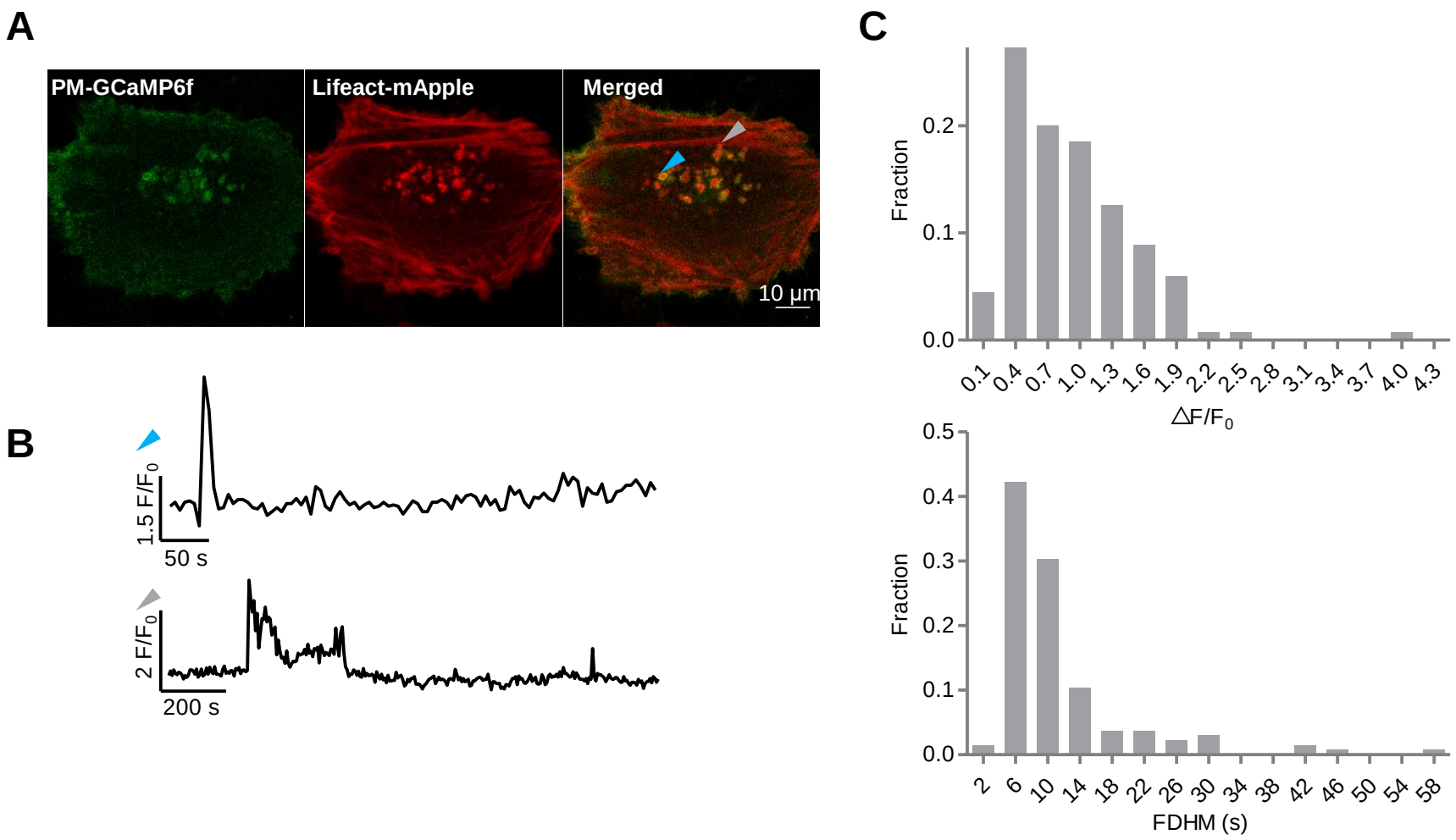

Fig. S1. Properties of PM-GCaMP6f-reported Ca^{2+} glows in WM793 cells.

A, PM-GCaMP6f expression and distribution in a representative cell. From left to right, confocal image of PM-GCaMP6f, invadopodia visualized by Lifeact-mApple fluorescence, and their merged images. **B**, Representative time courses of PM-GCaMP6f-reported invadopodial Ca^{2+} glows. **C**, Histograms of amplitude and duration of PM-GCaMP6f Ca^{2+} glows (n = 135 events from 18 cells, N = 12 independent experiments).

Fig. S2

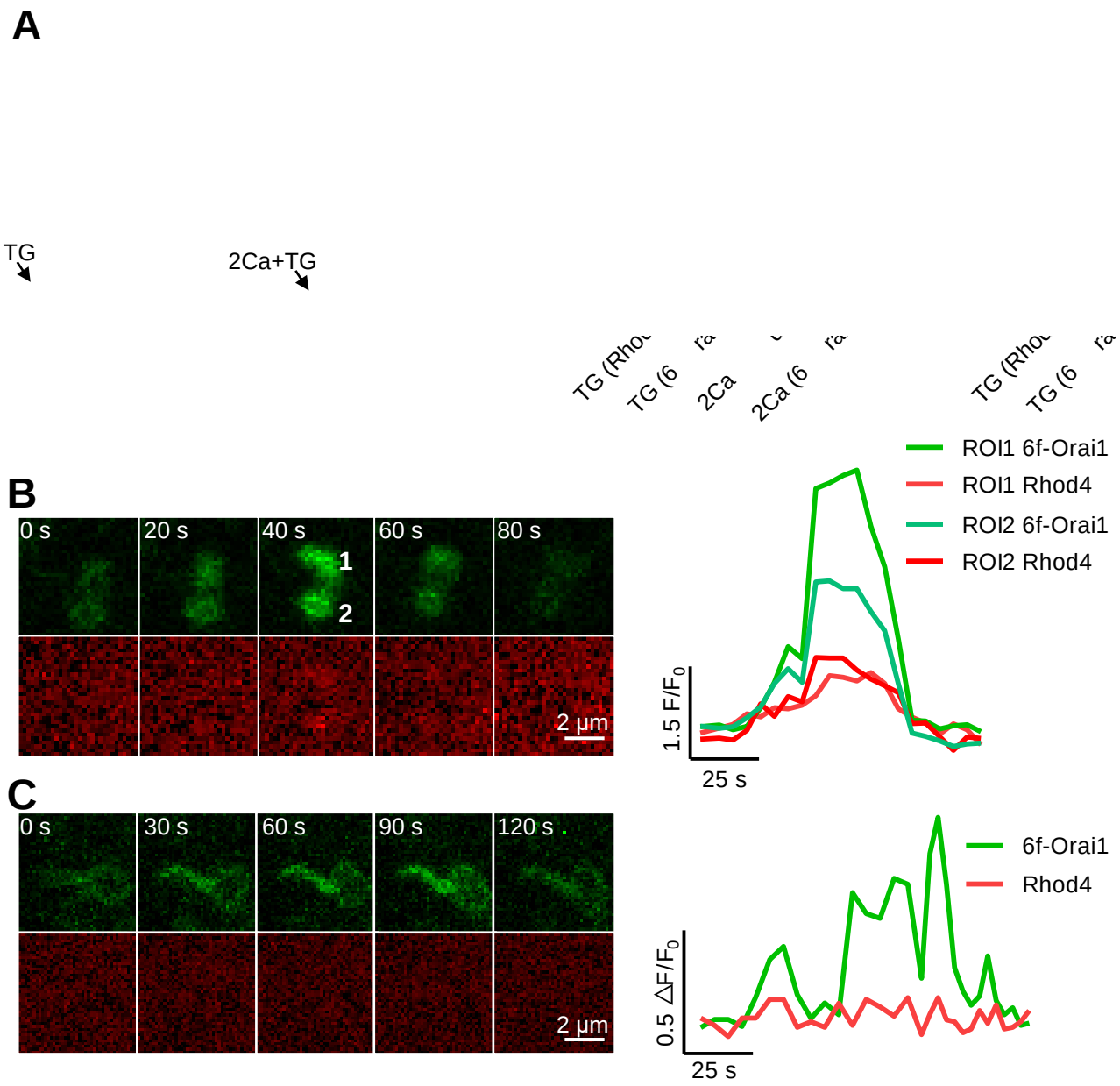

Fig. S2. Comparison of GCaMP6f-Orai1 and Rhod4 sensitivity to Ca^{2+} influx and release flux.

A, Typical time courses (left) and average amplitude (middle) and duration (right) of simultaneously-recorded Rhod4 and GCaMP6f-Orai1 fluorescence responding to 5 µM thapsigargin (TG) followed by recovery with 2 mM Ca^{2+}. During SOCE, GCaMP6f-Orai1 and Rhod4 transients displayed similar amplitudes and kinetics. During TG-induced ER release, however, the GCaMP6f-Orai1 transient had a smaller amplitude and abbreviated duration (n = 30 cells from 8 independent experiments). **B** and **C**, Confocal images of invadopodial Ca^{2+} glows measured with GCaMP6f-Orai1 and Rhod4. The corresponding traces from selected invadopodia are shown to the right. While GCaMP6f-Orai1 registered robust Ca^{2+} glows, Rhod4 glows were rather weak (**B**) or indiscernible (**C**). Data represent mean ± SEM; ***p <0.001; NS, not statistically significant.

Fig. S3

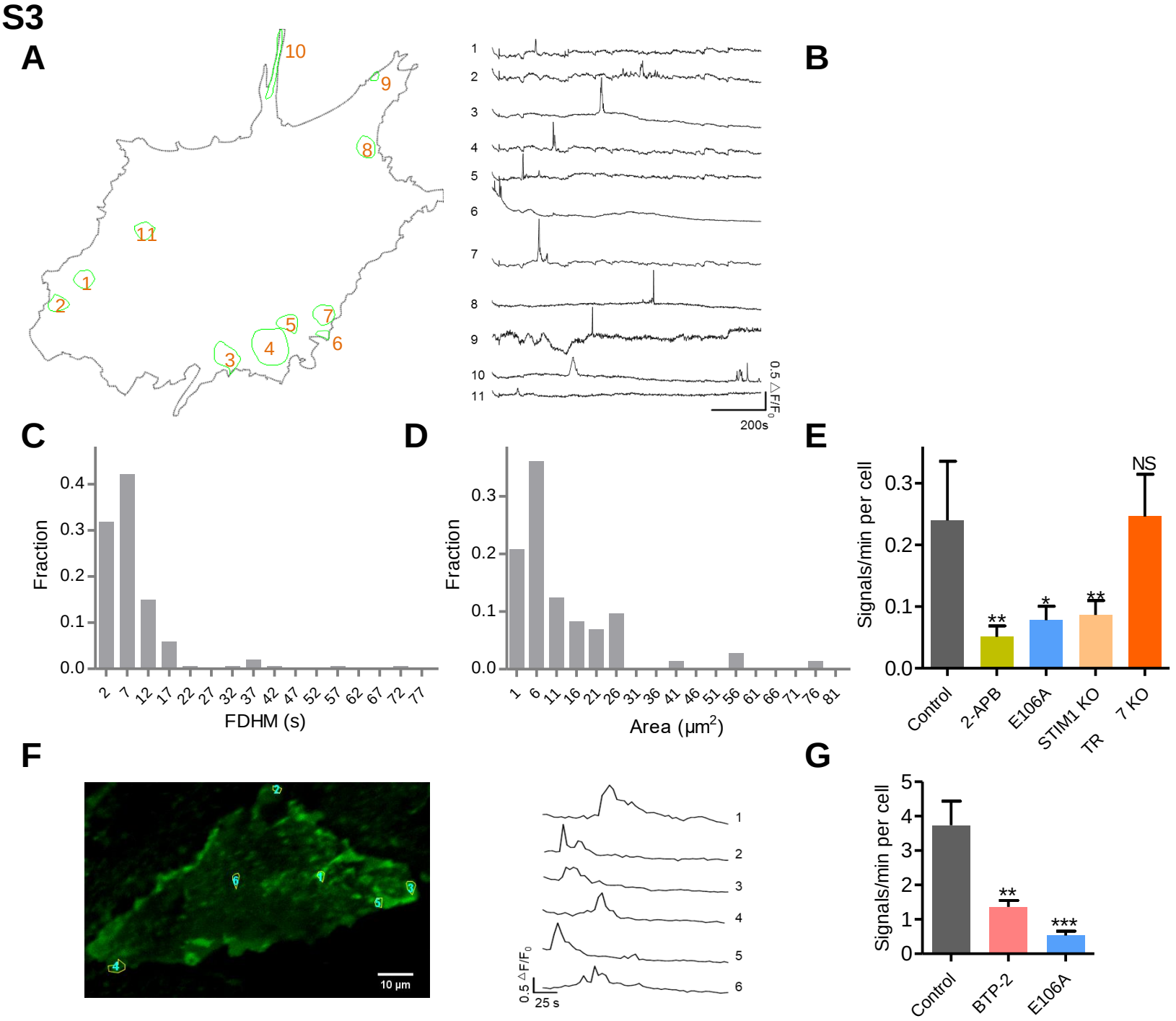

Fig. S3. Peripheral Ca^{2+} glows in WM793 cells and Ca^{2+} glows in HUVECs.

A, Map of the firing sites of extra-invadopodial glows and the corresponding traces from the numerically labeled regions (see Fig 2A legend for experimental conditions). **B**, **C**, and **D**, Histograms of amplitude (**B**), duration (**C**), and area (**D**) of spontaneous Ca^{2+} glows (n = 154 events from 16 unstimulated cells). **E**, Frequencies of peripheral Ca^{2+} glow under different experimental conditions (n = 16, 18, 21, 36, and 15 cells from 13, 8, 16, 25, and 12 independent experiments for control, 2-APB, E106A, STIM1 KO, and TRPM7 KO, respectively. **F**, Ca^{2+} glows from a HUVEC expressing GCaMP6f-Orai1. HUVECs were infected with GCaMP6f-Orai1 adenovirus for 36 h, then treated with 50 ng/mLVEGF for 3 h and were subjected to confocal imaging for 400 s at 0.8 s/frame with 4-s interval. Left, a HUVEC stained with GCaMP6f-Orai1. Right, representative time courses corresponding to local areas marked by numbers in the left panel. G, Statistics showing the frequency of Ca^{2+} glows in Control (n = 9 cells from N = 5 independent experiments), 5 μM BTP2-treated (n = 13, N = 5), and Orai1-E106A (n = 11, N = 6) HUVECs. Data are presented as mean ± SEM; *p <0.05, **p <0.01, ***p <0.001 compared to control; NS, not statistically significant.

Fig. S4

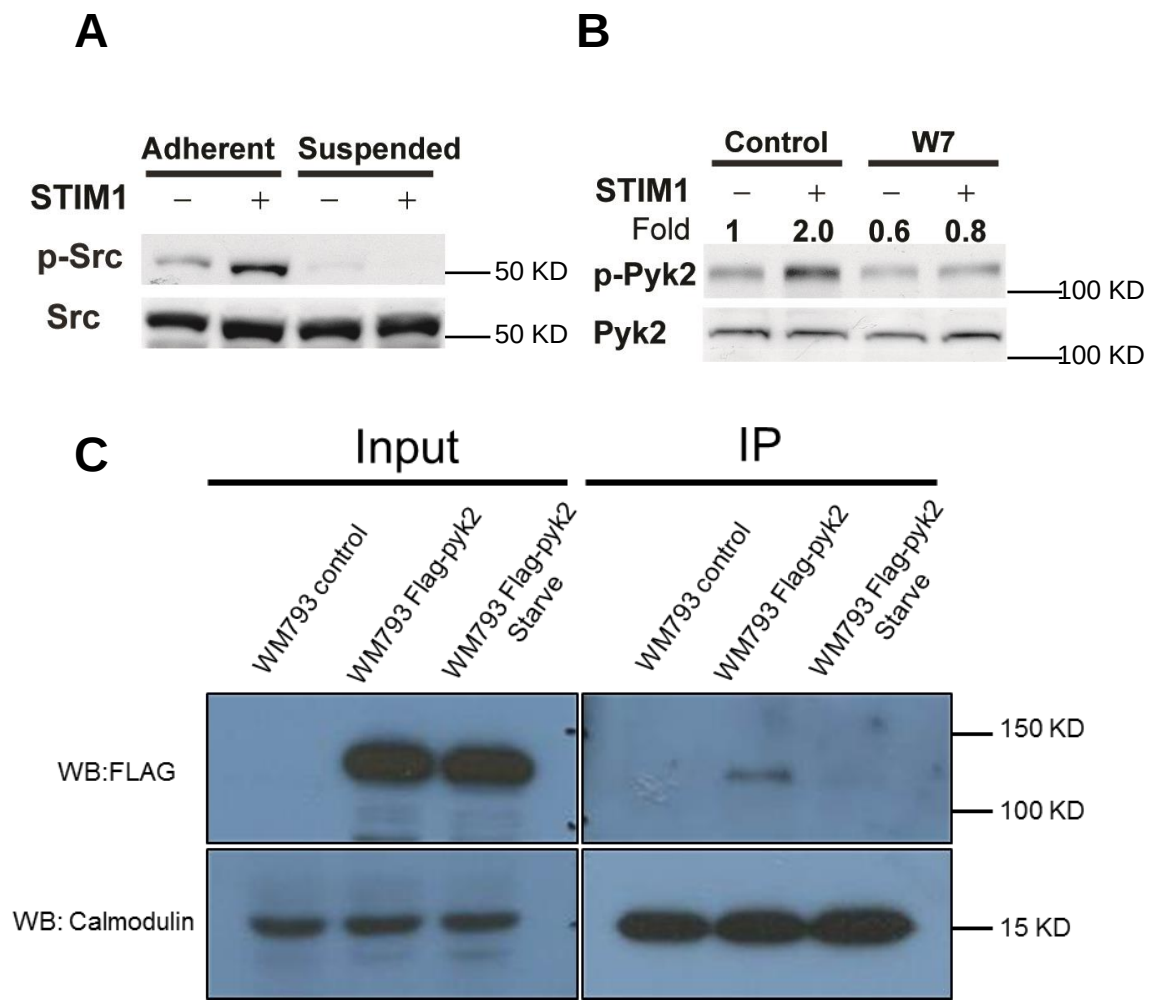

Fig. S4. Calmodulin interacts with Pyk2 during invadopodial formation.

A, Western blots showing that cell adhesion was required for STIM1-mediated activation of Src.

B, Inhibition of calmodulin with W7 (20 μM) abolished the STIM1-mediated activation of Pyk2.

C, Co-immunoprecipitation showing Pyk2 interacts with calmodulin during invadopodial formation. Note that 'WM793 Flag-Pyk2 starve' indicates WM793 cells transfected with Flag-Pyk2 but not exposed to 10% FBS that is required to initiate the growth of invadopodia.

Data are representative results from at least 3 independent experiments.

Fig. S5

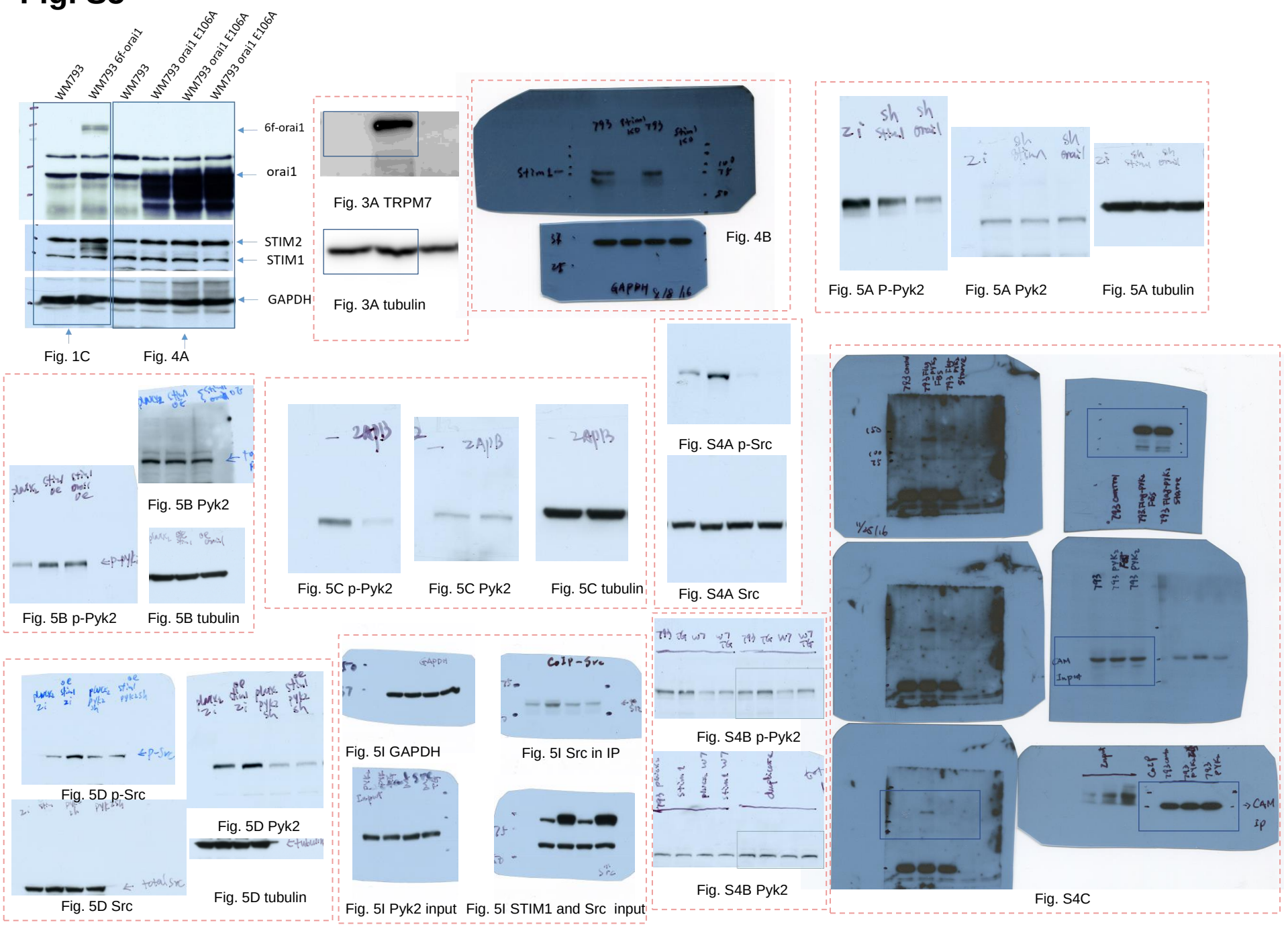

Fig. S5. Unprocessed scans of original blots shown in the main text and supplementary figures

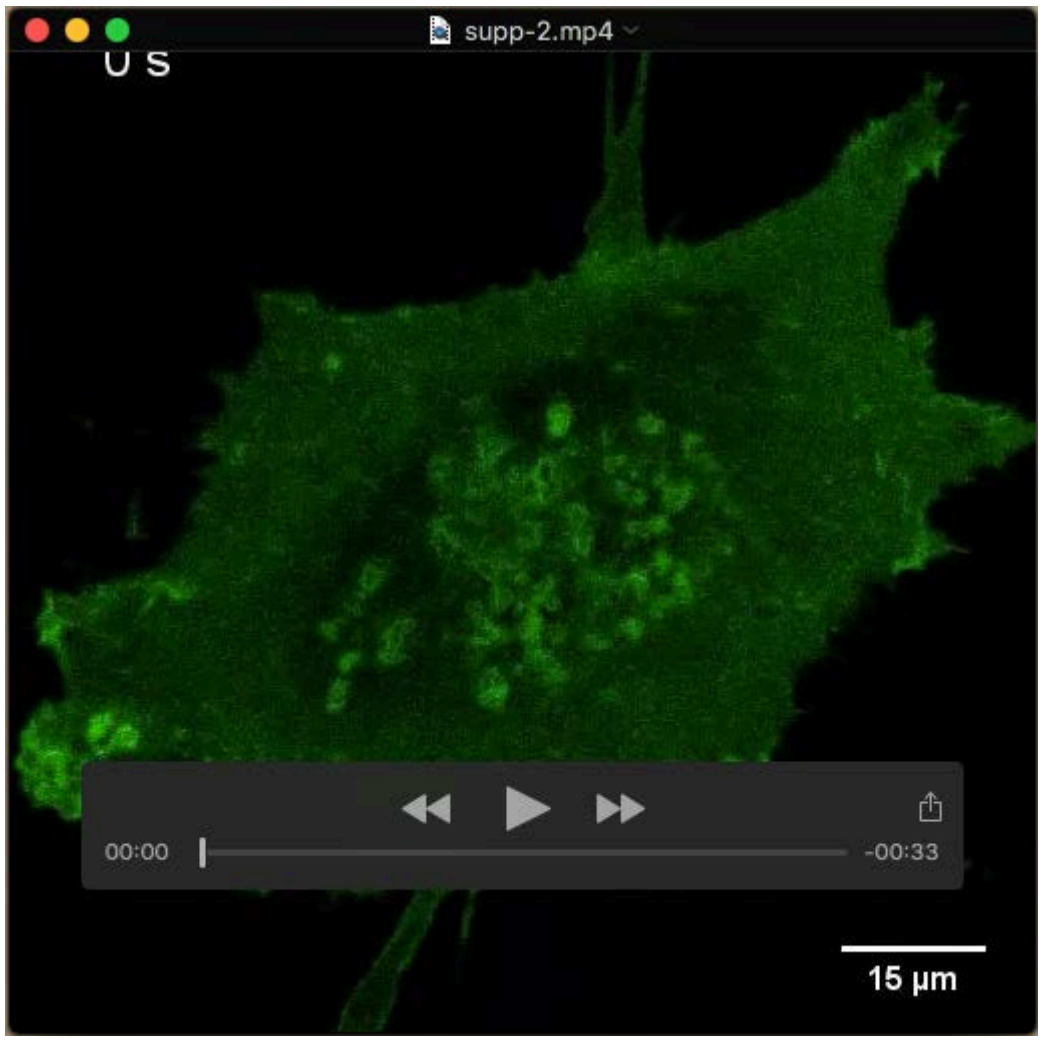

Movie 1. Spontaneous SOCE Ca^{2+} glows in WM793 cells

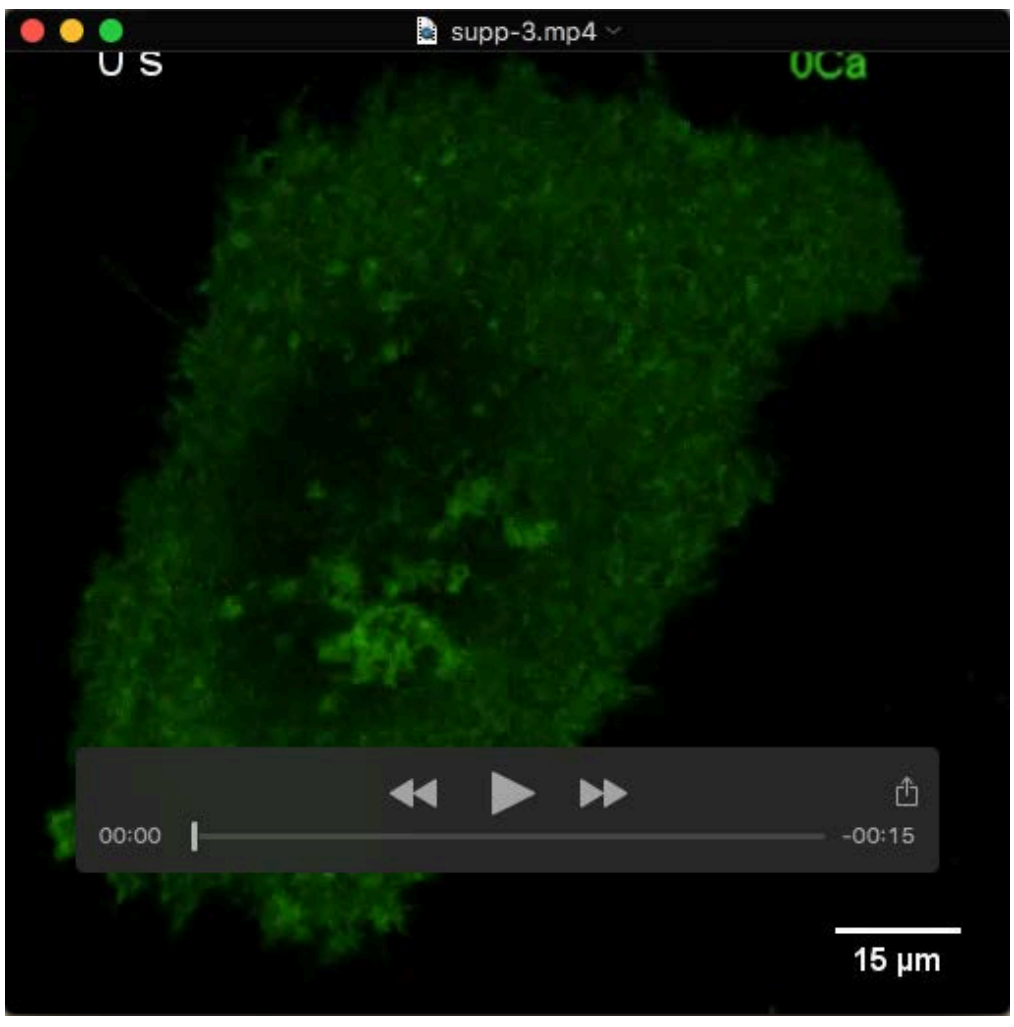

Movie 2. SOCE Ca^{2+} glow activity during store depletion and external Ca^{2+} re-addition